Supplementary Information (SI) for Journal of Materials Chemistry A.

Supporting Information

Crystal size/strain modulation and balanced electrochemical activity regulate the water oxidation performance of hematite photoanodes

Triet Thien Huu Nguyen[1], James Murphy[1], Gabriel Aygur[1], Edwin Mayes[2], Billy James Murdoch[2], Joel van Embden[1], Daniel Gómez[1], Enrico Della Gaspera[1]

[1] School of Science, RMIT University, Melbourne VIC 3001, Australia.
[2] RMIT Microscopy and Microanalysis Facility, College of Science, Engineering and Health, RMIT University, Melbourne, VIC 3000, Australia.

Corresponding author: * enrico.dellagaspera@rmit.edu.au

1. Experimental Methods

Preparation of substrates

FTO/glass (NSG TEC7, ≈7 Ω/□) was cut into 3.0 cm x 1.5 cm pieces, then carefully cleaned with sponge and detergent, and rinsed with distilled water. Then the FTO substrates were ultrasonically cleaned in Milli-Q water, ethanol, acetone, and isopropyl alcohol (IPA) for 10 minutes each. Finally, the substrates are dried with a gentle stream of N_2 before usage.

Preparation of precursor solution

0.404 g of iron (III) nitrate nonahydrate ($Fe(NO_3)_3.9H_2O$, Sigma-Aldrich, 98%) was added into 50 mL Milli-Q water in a centrifuge tube and sonicated in ice cold water until dissolved, yielding 20 mM Fe^{3+} solution. The tube containing the precursor solution was then taken out of the sonicator, and rested until reaching room temperature before spray coating. For doped precursor solution, an appropriate amount of stock dopant (2 M Ti or 2 M F) solutions was added the undoped precursor solution.

F stock solution was prepared by adding 0.1482 g ammonium fluoride (NH_4F, Sigma Aldrich, 99.99%) into 2 mL Milli-Q water, stirred using a magnetic stir bar for 20 minutes, yielding a total of 2 mL of 2 M NH_4F solution. Diammonium dihydroxybis(lactato)titanate(2-) ($[CH_3CH(O^-)CO_2NH_4]_2Ti(OH)_2$, Sigma Aldrich, 50% wt in H_2O) already has a molarity of 2 M, hence it was used as is.

Fabrication of α-Fe_2O_3 photoanodes

Nadetech ND-SP ultrasonic spray coater with a 90 kHz nozzle was used to deposit α-Fe_2O_3 on FTO substrates. FTO substrates were placed on a hotplate set at 400 °C for at least 5 minutes prior to deposition. A thin strip of cut silicon wafer was placed on top at the edge of the FTO substrate to block that area from the deposition of hematite, allowing it to be used for electrical contact in photoelectrochemical (PEC) measurements later. The nozzle position and movement are controlled by the software. The nozzle was set to be 12 cm away from the hot plate surface, and moving at a speed of 600 mm/min, with a flow rate of 60 mL/h. To produce highly uniform hematite thin films, spray coating was done in a raster pattern, where the nozzle first moves in a straight line in the x-direction along the length of the FTO substrate, then shifted by 1 mm in the y-direction along its width, and repeated for 16 times for a single layer. This produces films of ≈275 nm in thickness. A second layer was deposited the same way to build up more film thickness while ensuring it to be free of pin holes. To fabricate thinner hematite films, the flow rate can be reduced accordingly.

Hematite samples were then annealed in a muffle furnace in air at 500 °C for 2 hours with a ramp rate of 8 °C/min, and cooled down naturally. For nitrogen annealing, the air annealed samples were then further annealed in a tubular furnace under high N_2 flow rate at 500 °C for 2 hours, then at 700 °C for only 10 minutes with a ramp rate of 10 °C/min, to avoid FTO substrate deformation.

Characterization techniques

X-Ray Diffraction (XRD) analysis was conducted using a Bruker D8 diffractometer with Cu-Kα operating at a voltage of 40 kV and a current of 40 mA. $K\alpha_2$ was subtracted and underlying FTO peaks were aligned and used as internal reference before further analysis. UV-Visible absorption (UV-Vis) measurements were done using an Agilent Cary 5000 UV-VIS-NIR spectrophotometer equipped with an integrating sphere. X-Ray Photoelectron Spectroscopy (XPS) was conducted on a Kratos Axis Supra spectrometer equipped with a concentric hemispheric electron analyzer, using monochromated Al Kα X-ray source (E_{hv} = 1486.7 eV). All spectra were calibrated using adventitious carbon C 1s at 284.8 eV. Scanning Electron Microscopy (SEM) images were taken using FEI Verios 460L XHR-SEM to study surface and cross-section morphology. Elemental composition was determined via Electron Dispersive X-ray Spectroscopy (SEM-EDS) using an Oxford Xmas 30 EDS detector in the same microscope. High Resolution Transmission Electron Microscopy (HR-TEM) images were captured using JEOL F200 CFEG TEM instrument operating at 200kV equipped with a Gatan Rio16 camera.

Photoelectrochemical measurements

Metrohm Autolab PGSTAT204 potentiostat equipped with FRA32 impedance analyzer module was used to perform photoelectrochemical (PEC) measurements. A typical 3-electrode configuration was used, where the hematite photoanode were mounted on the outside of a custom-made PEC cell, a Pt coiled wire as the counter electrode and Hg|HgO|1 M KOH [Corrtest, CS902] as the reference electrode. The photoanode was illuminated from the back using AM1.5G simulated sunlight. The aperture of the PEC defined the working the active area of 0.45 cm^2. 1 M potassium hydroxide (KOH) with pH ≈ 13.7 was used as electrolyte. In some experiment, 1 M sodium sulfite (Na_2SO_3, Sigma-Aldrich, 98%) was added to the 1 M KOH electrolyte to act as hole scavenger.

Linear Sweep Voltammetry (LSV) was conducted to measure PEC water splitting performance, with applied potentials from -0.3 $V_{Hg|HgO}$ to +0.7 $V_{Hg|HgO}$, and a scanning rate of 10 mV/s. To convert applied potential from V versus Hg|HgO ($V_{Hg|HgO}$) to Reversible Hydrogen Electrode (V_{RHE}), use the following equation:

$$V_{vs\ RHE} = V_{vs\ \mathrm{Hg|HgO}} + V^{\mathrm{O}}_{\mathrm{Hg|HgO}\ vs\ RHE} + 0.059 \cdot pH$$

The standard reference electrode potential $V^{\mathrm{O}}_{\mathrm{Hg|HgO}\ vs\ RHE} = 0.120(V)$ at 25°C was obtained by measuring open circuit potential with a known Ag|AgCl|KCl (3 M saturated with AgCl, eDaq ET073) reference electrode.

Electrochemical Impedance Spectroscopy (EIS) measurements were conducted under solar illumination at 1.23 V_{RHE} in 1 M KOH (without hole scavenger) using AC voltage with amplitude of 10 mV RMS and frequency range of 100 kHz – 10 mHz. To obtain measurements at multiple applied potentials, the process is repeated from -0.3 $V_{Hg|HgO}$ to +0.7 $V_{Hg|HgO}$ with a step size of 25 mV, with 5 minutes of relaxation between applied potentials. An appropriate equivalent circuit $R_s([R_{bulk}(R_{surf}C_{surf})]C_{bulk})$ was fitted to all Nyquist plots using Metrohm Nova software to extract resistances and capacitances.[1] Constant phase element Q was used in place of capacitance C to enable good fit.

Cobalt phosphate (Co-Pi) cocatalyst was deposited by photo-assisted electrodeposition adapted from the literature.[2] In short, 0.1 M phosphate solution with pH ≈ 7 was prepared from by dissolving potassium phosphate dibasic (HK_2PO_4, Sigma-Aldrich, 98%) and potassium phosphate monobasic (H_2KPO_4, Sigma-Aldrich, 99%) in Milli-Q water. Then 0.5 mM cobalt (II) nitrate hexahydrate ($Co(NO_3)_2.6H_2O$, Sigma-Aldrich, 98%) was added to the phosphate solution and shaken vigorously. The photo-assisted electrodeposition was conducted using chronoampetrometry (CA) at 1.23 V_{RHE} until 3.6 mC/cm^2 were used, using the same PEC setup above.

2. Calculation of bulk charge transport and surface charge transfer efficiencies

The photocurrent density j of a photoanode is given by:

$$j = j_{Abs} \cdot \eta_{bulk} \cdot \eta_{surf}$$

Where:

j_{Abs}	is the maximum photocurrent density if all absorbed photons are converted to photogenerated electrons/holes, (in mA/cm^2).
η_{bulk}	is the charge transport efficiency in the bulk.
η_{surf}	is the charge transfer efficiency on the surface.

It is obvious that when measured in presence of a hole scavenger such as Na_2SO_3, the charge transfer efficiency on the surface η_{surf} becomes 1. Thus:

$$\eta_{bulk} = \frac{j_{\mathrm{Na_2SO_3}}}{j_{Abs}}$$

$$\eta_{surf} = \frac{j_{\mathrm{KOH}}}{j_{\mathrm{Na_2SO_3}}}$$

The maximum photocurrent density j_{Abs} can be calculated according to:

$$j_{Abs} = \int_0^{\lambda_g} \phi_{solar}(\lambda)\left(1 - 10^{-Abs(\lambda)}\right) q_e d\lambda$$

Where:

$\phi_{solar}(\lambda)$	is the AM1.5G solar spectral photon flux, (in mHz/cm^2/nm).
$Abs(\lambda)$	is the absorbance due to light absorption of the photoanode.
λ	is the wavelength of photon, (in nm).
q_e	is the elementary charge, (in C).
h	is the Planck constant, (in Js).
c	is the speed of light in vacuum, (in m/s).
λ_g	is the onset wavelength of sprayed coated hematite samples, (in nm).

3. Halder-Wagner analysis

The shape of a peak in X-ray diffractogram is a convolution of Lorentzian (influenced by crystallite size D) and Gaussian (influenced by microstrain ε) functions. Halder-Wagner equation relates these two quantities by the following equation:[3,4]

$$\left(\frac{\beta\cos(\theta)}{\sin(\theta)}\right)^2 = \frac{K\lambda}{D}\frac{\beta\cos(\theta)}{\sin^2(\theta)} + 16\varepsilon^2$$

Where:

β	is FWHM of the Voigt fit of the peak, (in radians).
θ	is half position of the Voigt fit of the peak, (in radians).
$K = 0.9$	is the shape factor.
λ	is X-ray wavelength, (in nm).
D	is the crystallite size, (in nm).
ε	is the microstrain of the lattice.

It is clear that the peak half position θ and FWHM β strongly influence the result of the analysis. Therefore, it is crucial to correct the diffractogram by aligning FTO peaks and eliminating $K\alpha_2$ prior to Halder-Wagner analysis. Furthermore, instrument broadening must be removed from the measured FWHM to obtain the correct sample FWHM β:

$$\beta^2 = \beta_{meas}^2 - \beta_{inst}^2$$

Instrument broadening was obtained by measuring a corundum Al_2O_3 reference standard (NIST1976C) under the same condition. Because corundum has different peak positions 2θ compared to hematite, quadratic regression of the plot of β versus 2θ ($R^2 \approx 0.98$) determined from corundum measurement was used to calculate β at 2θ of hematite:

$$\beta_{inst} = A(2\theta)^2 + B(2\theta) + C$$

We must also note that in the paper by Dolabella,[3] and the original paper by Halder and Wagner,[4] integral breadth was chosen instead of FWHM to measure the breadth of the peak. In our case, since both approaches yielded practically identical result, we believe that using FWHM is reasonably accurate.

4. Modelling of electrochemical impedance spectroscopy (EIS) data

Since two semicircles can be clearly identified from Nyquist plots, the equivalent circuit $R_s([R_{bulk}(R_{surf}C_{surf})]C_{bulk})$ was chosen, where C_{bulk}, C_{surf} are capacitances of bulk charge transport and surface charge transfer processes respectively, while R_s, R_{bulk}, R_{surf}, are resistances of electrolyte/contact/wire, bulk charge transport and surface charge transfer processes respectively.[1]

However, because of non-ideal behavior of capacitor C, constant phase element Q must be substituted to enable a good fit with experimental data. To estimate the average capacitance C of an (RQ) loop, one can use the following formula:[5,6]

$$C = Y_0^{\frac{1}{N}} \left(\frac{1}{R}\right)^{\frac{N-1}{N}}$$

Where Y_0 is the magnitude, $0 \leq n \leq 1$ is the extent of capacitor behavior. The formula works well for the inner ($R_{surf}Q_{surf}$) loop, allowing us to estimate C_{surf} accurately. However, this formula is not strictly accurate to calculate the C_{bulk} because the formula does not account for impedance of ($R_{surf}C_{surf}$) connected in series with R_{bulk}.

The characteristic time constant τ of an (RC) loop is the product of the resistance R and capacitance C:[5]

$$\tau = RC$$

Hence, one can estimate the time constant of the surface charge transfer process τ_{surf}, by multiplying R_{surf} and C_{surf} calculated earlier. The larger the time constant, the slower the charge transfer process and vice versa.

5. Supplementary Figures

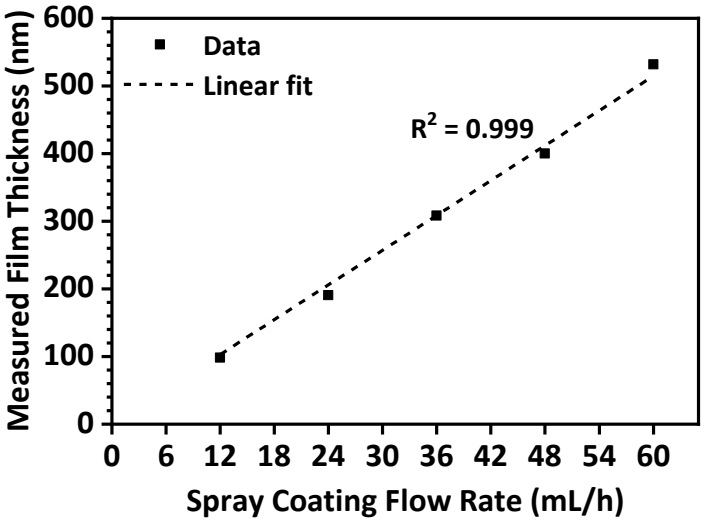

Figure S1. Hematite film thickness measured from cross-section SEM as a function of spray flow rate.

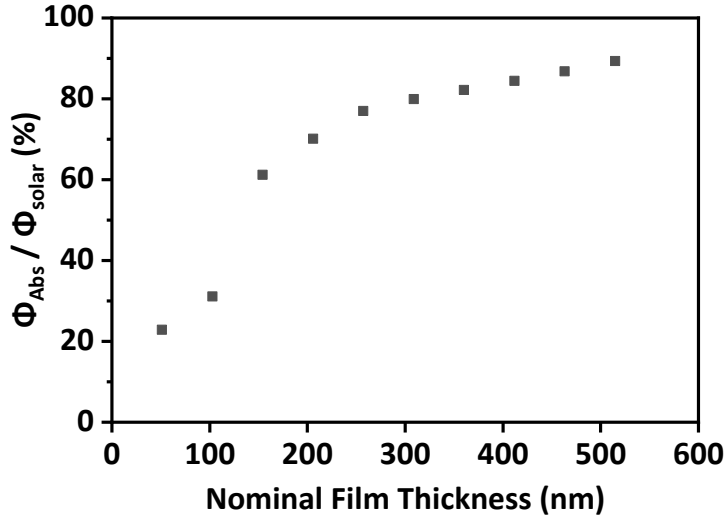

Figure S2. Fraction of solar photon flux (with energy above the hematite band gap) absorbed as a function of film thickness.

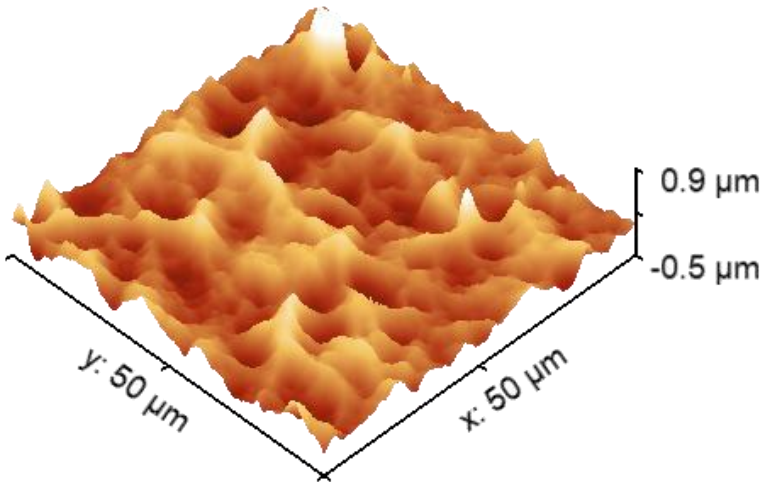

Figure S3. Surface AFM image of undoped hematite.

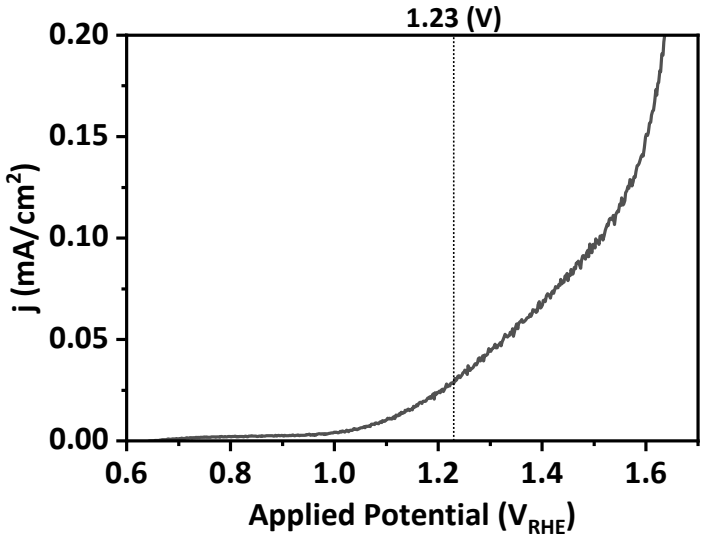

Figure S4. LSV plot of undoped hematite in 1M KOH electrolyte.

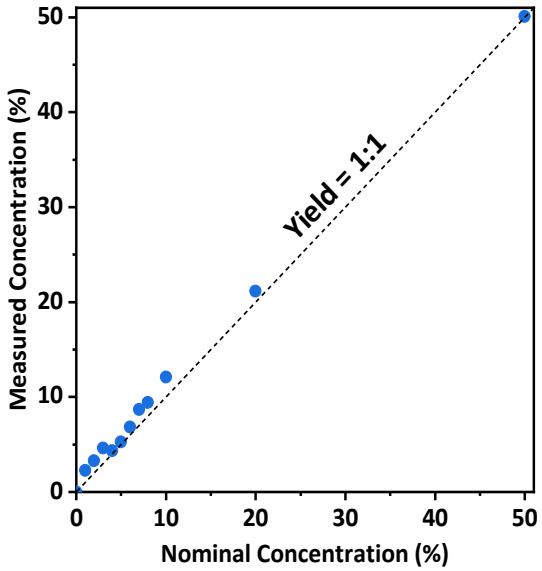

Figure S5. Atomic Ti concentration (Ti/(Ti+Fe)) measured from SEM-EDS versus nominal values.

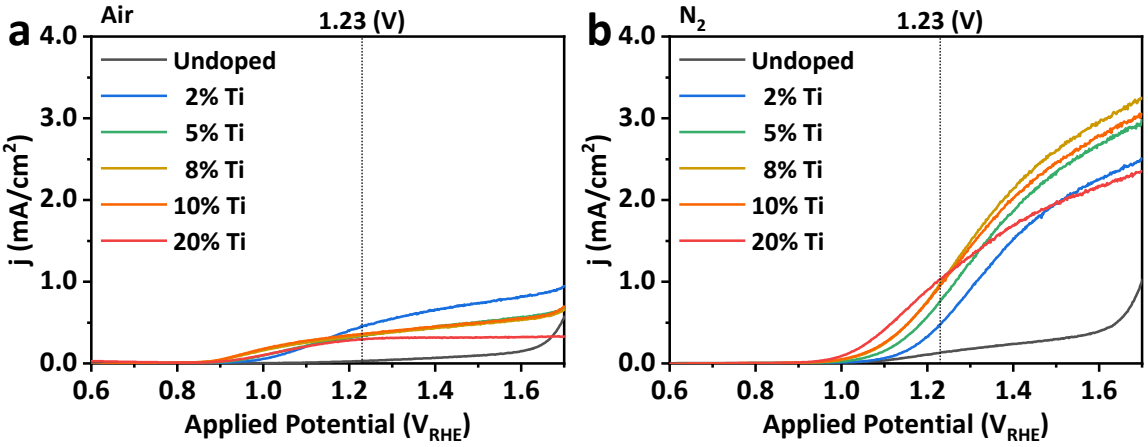

Figure S6. LSV plots of hematite doped with various Ti concentration before (a) and after (b) annealing in N_2.

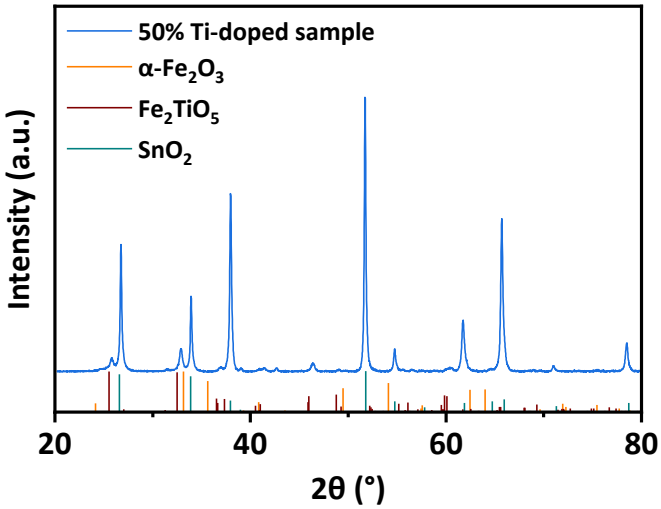

Figure S7. XRD pattern of 50% Ti-doped sample. Excessive Ti loading causes segregation of pseudo-brookite Fe_2TiO_5, while hematite α-Fe_2O_3 peaks become suppressed.

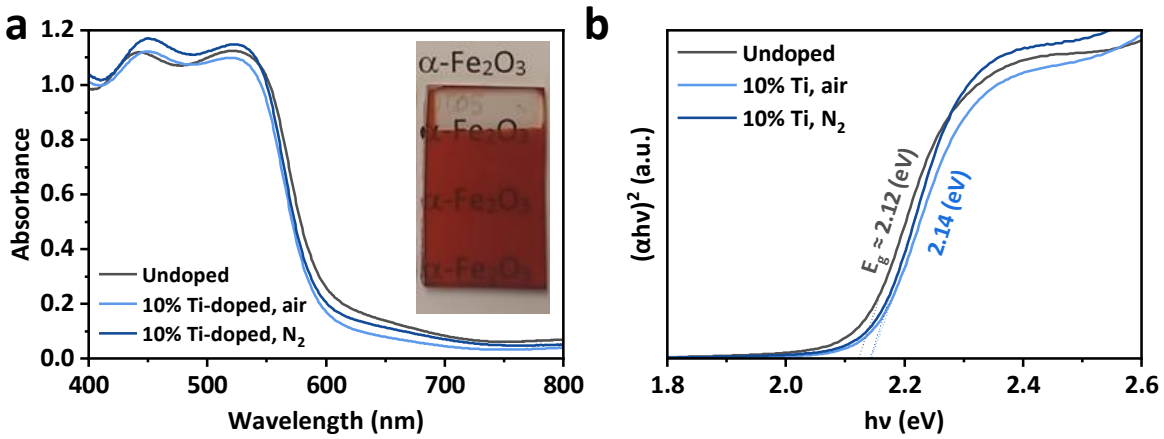

Figure S8. UV-Vis absorbance spectra (a) and Tauc plot (b) of various hematite films: undoped (black), 10% Ti-doped annealed in air (light blue), and annealed in N_2 (dark blue).

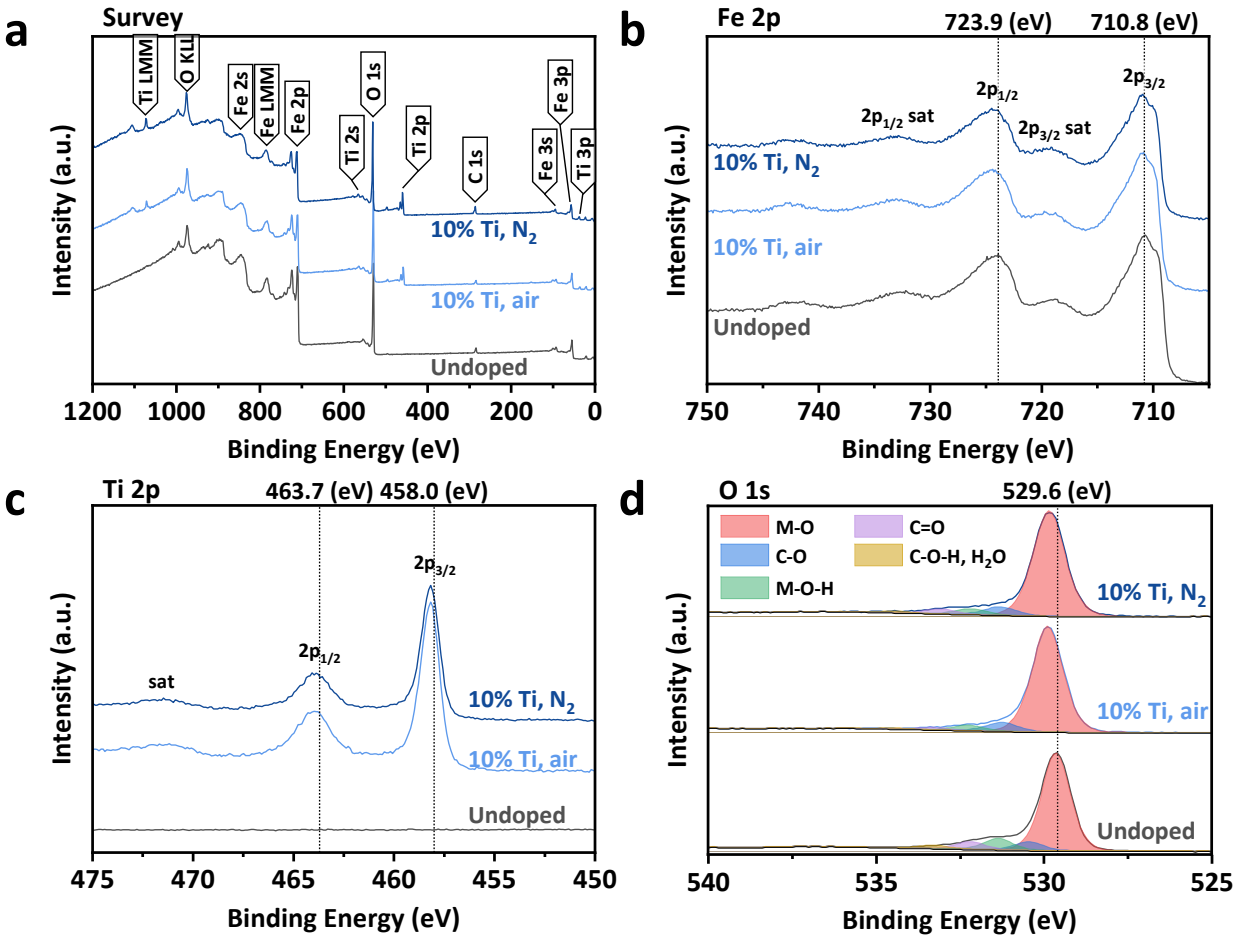

Figure S9. Survey (a), O1s (b), Fe2p (c), Ti2p (d) XPS spectra of various hematite films: undoped (black), 10% Ti-doped annealed in air (light blue), or N_2 (dark blue).

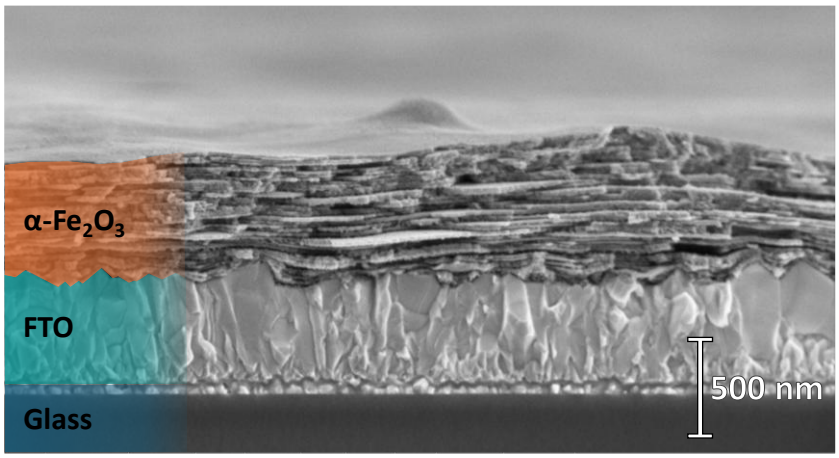

Figure S10. Cross-section SEM image of 10% Ti-doped sample deposited on a glass-FTO substrate.

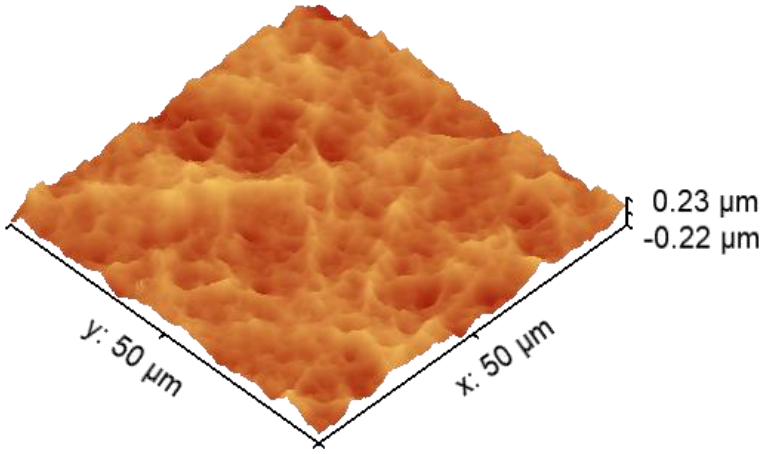

Figure S11. Surface AFM image of 10% Ti-doped sample.

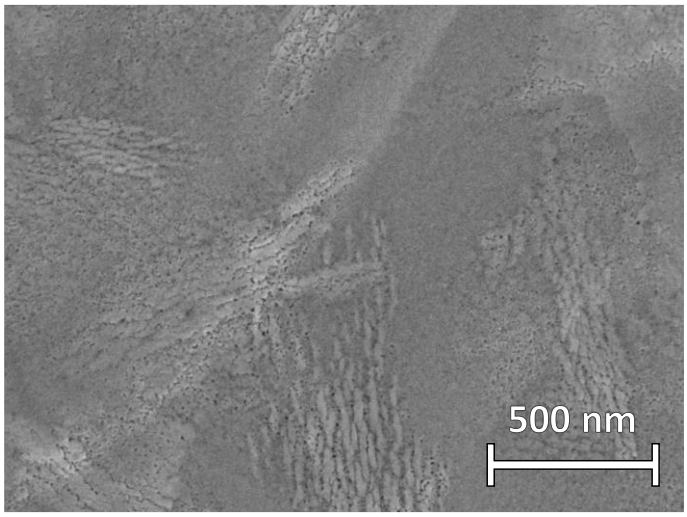

Figure S12. Surface SEM image of 10% Ti-doped sample.

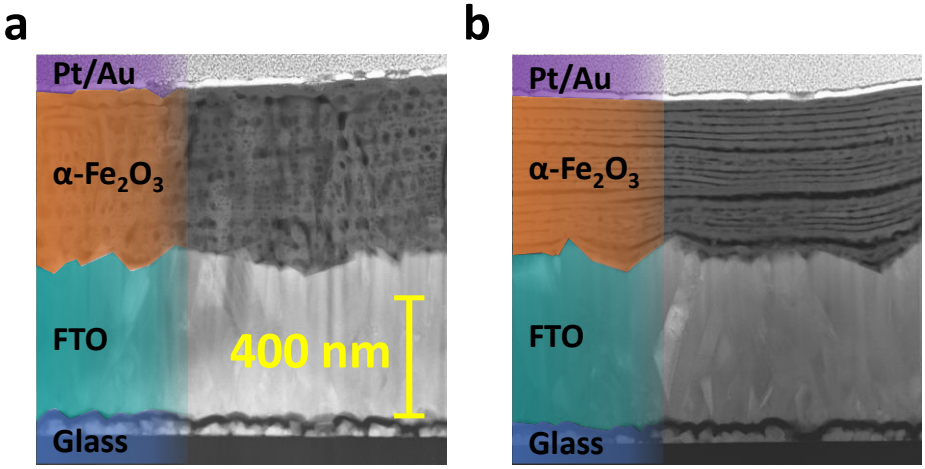

Figure S13. Zoomed out TEM images of cross-section of a) undoped, b) 8% Ti-doped N_2 annealed hematite samples.

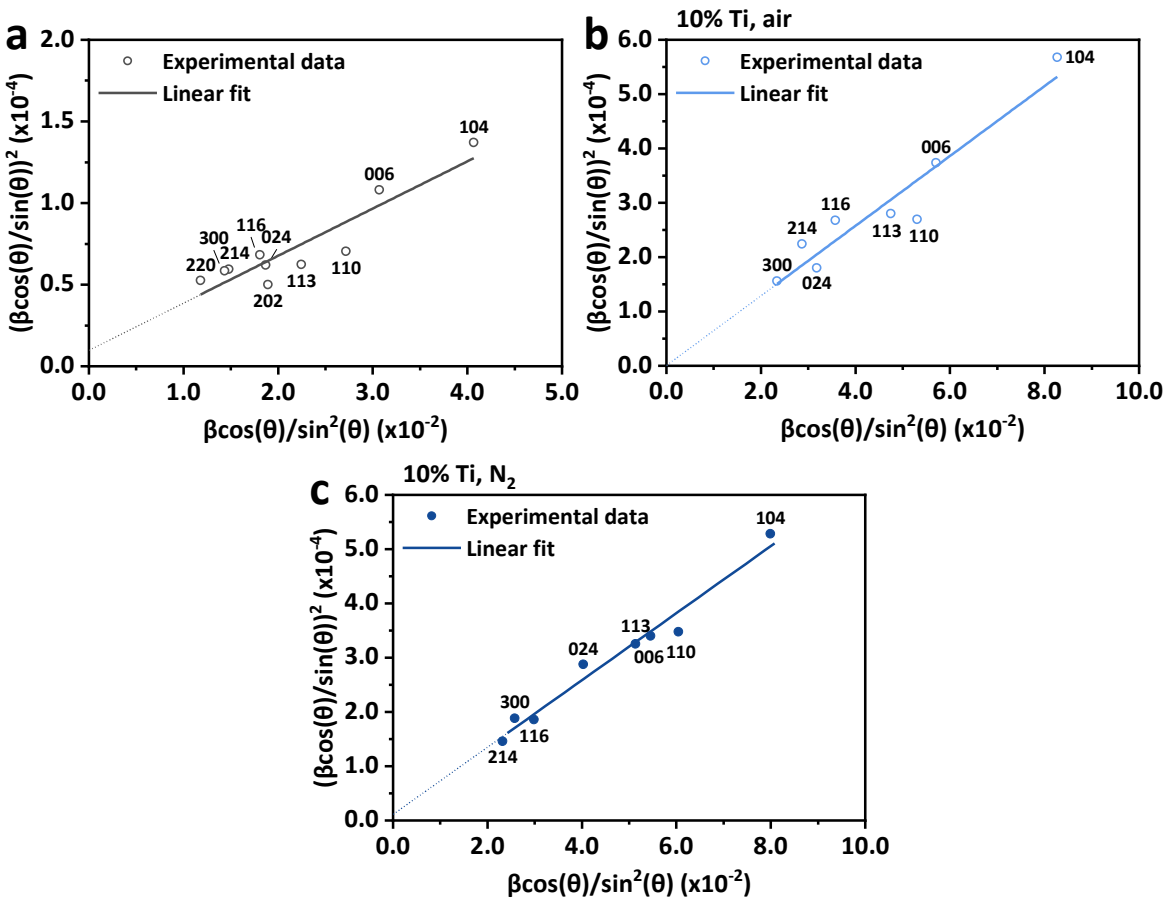

Figure S14. Halder-Wagner plots of undoped (a), 10% Ti-doped hematite annealed in air (b) or N2 (c).

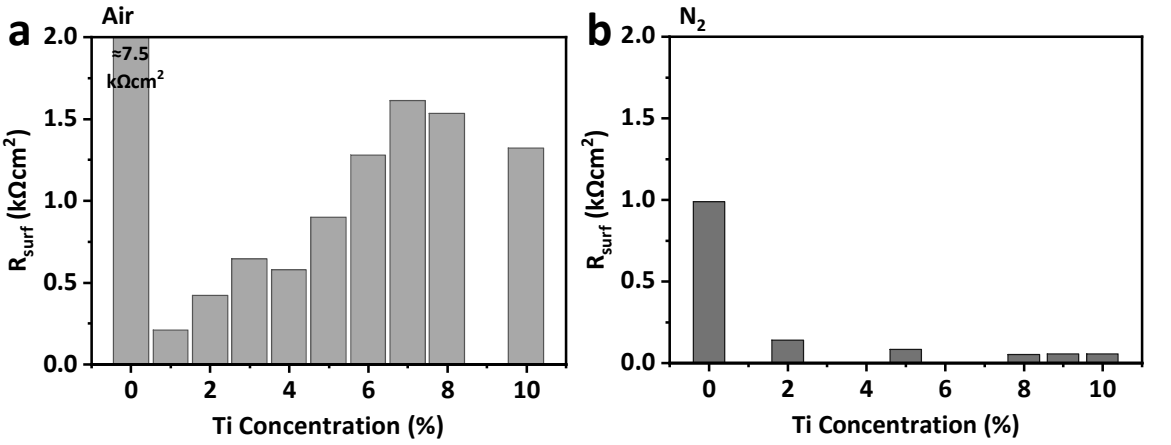

Figure S15. R_{surf} measured at 1.23 V_{RHE} as a function of Ti dopant concentration for hematite samples annealed in air (a) or in N_2 (b).

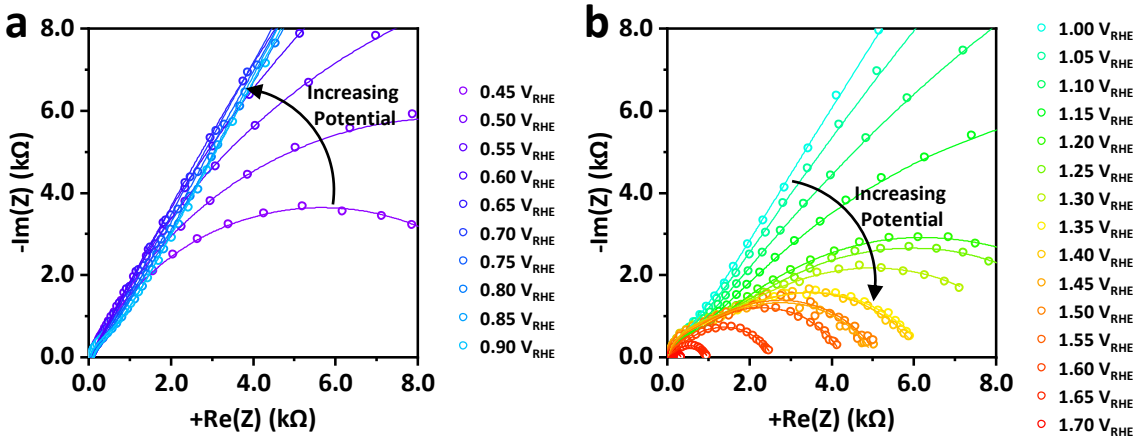

Figure S16. Nyquist plots of undoped hematite at various applied potentials under 1 Sun illumination.

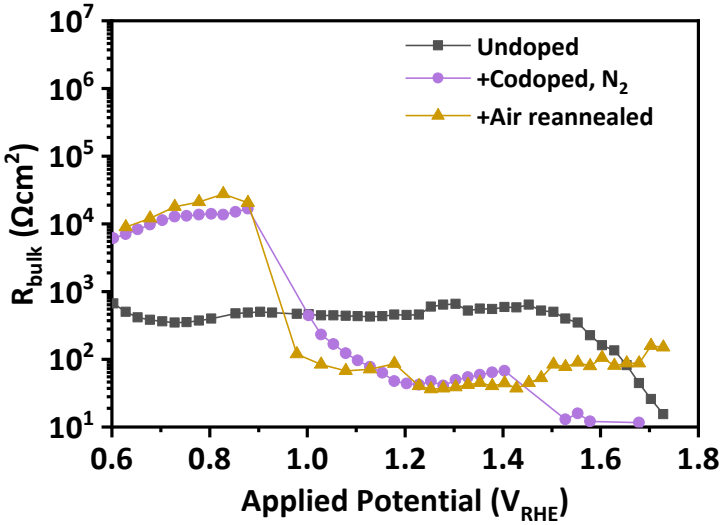

Figure S17. R_{bulk} as a function of applied potentials under 1 Sun illumination for key hematite samples.

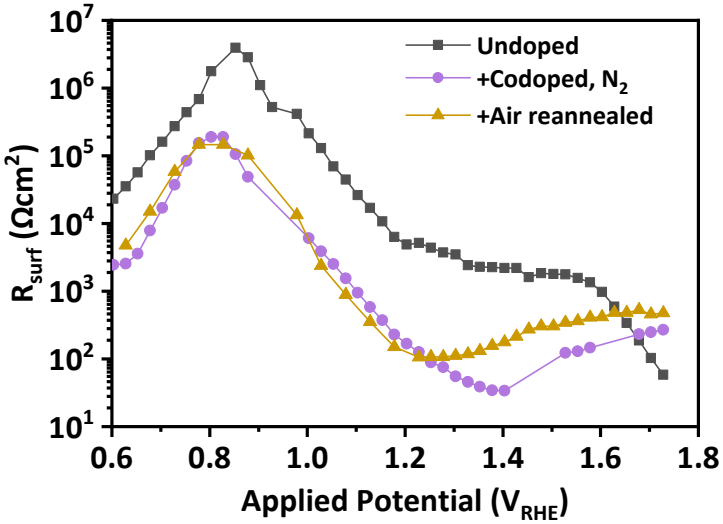

Figure S18. R_{surf} as a function of applied potentials for key hematite samples.

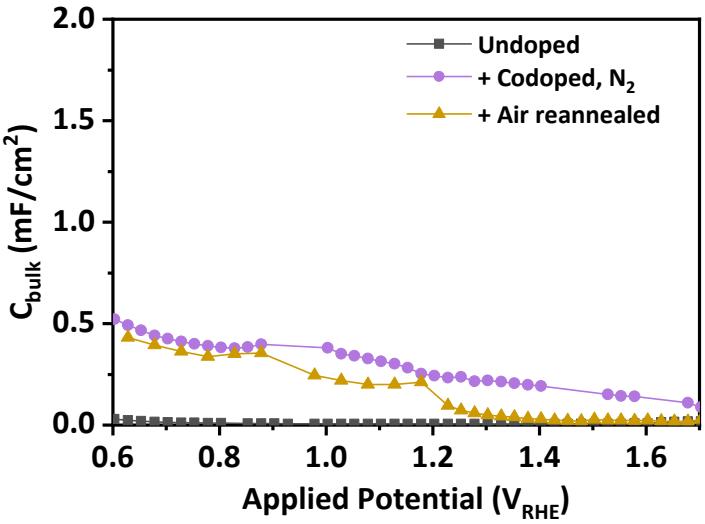

Figure S19. C_{bulk} as a function of applied potentials for key hematite samples.

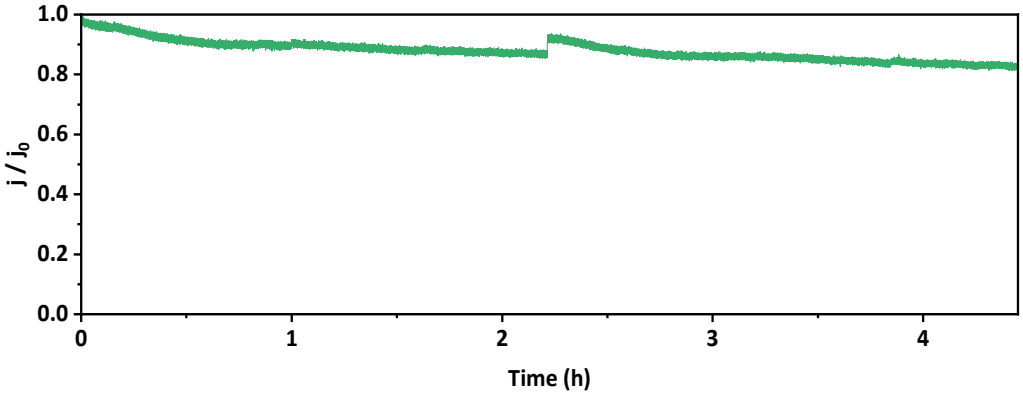

Figure S20. Relative photocurrent density at 1.23 V_{RHE} as a function of time for one of the top hematite samples. The spike at ~2h 15m is due to oxygen bubbles desorbing from the surface of the photoanode.

Table S1. Bulk charge transport resistance measured at 1.23 V_{RHE}, crystallite size and microstrain of key samples.

Sample	R_{bulk} (Ωcm^2)	D (nm)	$\|\varepsilon\|$ ($x10^{-3}$)
Undoped	509	47.9	0.785
+ 8% Ti-doped, N_2	69	24.9	1.800
+ 20% F-co-doped	42	23.0	1.800

Table S2. Surface charge transfer resistance, capacitance and time constant at the onset potential of key samples.

Sample	R_{surf} (Ωcm^2)	C_{surf} (F/cm^2)	τ_{surf} (s)
Undoped	4.0×10^6	1.5×10^{-3}	6.1×10^3
+ Codoped, N_2	3.9×10^1	1.2×10^{-3}	4.5×10^{-2}
+ Air reannealed	1.1×10^2	3.9×10^{-5}	4.2×10^{-3}

References

1 J. Li, W. Wan, C. A. Triana, H. Chen, Y. Zhao, C. K. Mavrokefalos and G. R. Patzke, Reaction kinetics and interplay of two different surface states on hematite photoanodes for water oxidation, *Nat Commun*, 2021, **12**, 255.

2 B. Klahr, S. Gimenez, F. Fabregat-Santiago, J. Bisquert and T. W. Hamann, Photoelectrochemical and Impedance Spectroscopic Investigation of Water Oxidation with "Co–Pi"-Coated Hematite Electrodes, *J. Am. Chem. Soc.*, 2012, **134**, 16693–16700.

3 S. Dolabella, A. Borzì, A. Dommann and A. Neels, Lattice Strain and Defects Analysis in Nanostructured Semiconductor Materials and Devices by High-Resolution X-Ray Diffraction: Theoretical and Practical Aspects, *Small Methods*, 2022, **6**, 2100932.

4 N. C. Halder and C. N. J. Wagner, Analysis of the Broadening of Powder Pattern Peaks using Variance, Integral Breadth, and Fourier Coefficients of the Line Profile, *Advances in X-Ray Analysis*, 1965, **9**, 91–102.

5 A. Ch. Lazanas and M. I. Prodromidis, Electrochemical Impedance Spectroscopy–A Tutorial, *ACS Meas. Sci. Au*, DOI:10.1021/acsmeasuresciau.2c00070.

6 G. J. Brug, A. L. G. van den Eeden, M. Sluyters-Rehbach and J. H. Sluyters, The analysis of electrode impedances complicated by the presence of a constant phase element, *Journal of Electroanalytical Chemistry and Interfacial Electrochemistry*, 1984, **176**, 275–295.